Water Supply

IWA PUBLISHING

Water Supply Vol 22 No 2, 1546 doi: 10.2166/ws.2021.334

Numerical analysis of hydrodynamics influenced by a deformed bed due to a near-bank vegetation patch

Zijing Yi[a,b], Yi Sun [c], Xiekang Wang [a], Daoxudong Liu [d] and Xufeng Yan [a,*]

[a] State Key Laboratory of Hydraulics and Mountain River Engineering, Sichuan University, Chengdu, China
[b] Undergraduate School, Chongqing University, Chongqing, China
[c] Yellow River Institute of Hydraulic Research, Zhengzhou, China
[d] Department of Civil and Environmental Engineering, The Hong Kong Polytechnic University, Hong Kong SAR, China
*Corresponding author. E-mail: xufeng.yan@scu.edu.cn

YS, 0000-0003-1258-3074; XW, 0000-0003-0065-404X; DL, 0000-0001-8081-6138; XY, 0000-0001-5540-8319

ABSTRACT

This study uses a 2D hydro-morphological model to analyze hydrodynamics over flat and deformed beds with a near-bank vegetation patch. By varying the patch density, the generalized results show that the hydrodynamics over deformed beds differs a lot from those over flat beds. It is found that the deformed bed topography leads to an apparent decrease in longitudinal velocity and bed shear stress in the open region and longitudinal surface gradient for the entire vegetated reach. However, the transverse flow motion and transverse surface gradient in the region of the leading edge and trailing edge is enhanced or maintained, suggesting the strengthening of secondary flow motion. Interestingly, the deformed bed topography tends to alleviate the horizontal shear caused by the junction-interface horizontal coherent vortices, indicating that the turbulence-induced flow mixing is highly inhibited as the bed is deformed. The interior flow adjustment through the patch for the deformed bed requires a shorter distance, L_a, which is related to the vegetative drag length, $(C_d a)^{-1}$, with a logarithmic formula ($L_a = 0.4\ln[(C_d a)^{-1}] + b$, with $b = 3.83$ and 4.03 for the deformed and flat beds). The sloping bed topographic effect in the open region accelerating the flow may account for the quick flow adjustment.

Key words: deformed bed topography, flow adjustment, inhibited shear layer development, near-bank patch

HIGHLIGHTS

- Near-bank vegetation results in a pool-riffle system.
- A 2D hydro-geomorphological model reproduced the deformed bed induced by near-bank vegetation.
- Hydrodynamics over flat and deformed beds are compared.
- Interior flow adjustment is shortened due to the formation of a deformed bed.
- Horizontally-dimensional turbulence is inhibited by the deformed bed.

1. INTRODUCTION

Vegetation widely occurs near banks of natural waterways such as rivers, channels and streams. The blockage of vegetation leads the original flow path to be modified, resulting in an evident reduction of flow velocity in the vegetated region but an increase in the adjacent open region (Rominger & Nepf 2011; Yan *et al.* 2016). The sediment transport pattern for the vegetation region is dominated by the depositional process and for the open region by the erosional process. With a mobile bed, the bed tends to aggrade in the vegetation region and tends to degrade in the open region. As a consequence, diverse bed forms are established around the near-bank vegetation. These bed forms are identified by pool, riffle and sediment bars (Kim *et al.* 2015; Xu *et al.* 2019). Together with seasonal flow variability, these bed forms provide habitats for different species (Xu *et al.* 2012; Santos *et al.* 2014; Zhao *et al.* 2015; Ghaderi *et al.* 2020) from the perspective of aquatic ecosystem restoration.

For a channel bed occupied by a near-bank vegetation patch, flow mass gets redistributed with more flow being directed to the adjacent open region. As a consequence, the flow in the open region accelerates with velocity increasing and in the

vegetated region decelerates with velocity decreasing. The junction of two regions forms significant flow shearing, which under a certain patch density tends to induce flow instability to resemble horizontal coherent vortices with pronounced turbulent activity. The coherent vortices continuously growing along the patch lead to the exchange of flow mass and momentum between the low-velocity vegetated region and high-velocity open region (Rominger & Nepf 2011; Nepf 2012; Yan *et al.* 2016). As the flow exits the vegetated reach, flow separation occurs, leading to the flow in the two regions recovering to a uniform pattern.

When the bed is erodible, bed scour in the open region adjacent to the patch is triggered as flow accelerates or bed shear stress increases. However, suspended loads tend to deposit in the vegetated region for flow deceleration. At equilibrium, the deformed bed topography exerts an effect on the hydrodynamics. With the same sediment size, the generated scour pool in the open region should alleviate the velocity and bed shear stress to prevent further bed erosion. Correspondingly, other hydrodynamic parameters associated with flow velocity, for instance, water surface gradient and turbulence, should also be influenced by the deformed bed topography. Therefore, the application of hydrodynamic knowledge of near-bank vegetated flows obtained for a flat bed may not be relevant for a deformed bed. Numerous studies have demonstrated the pronounced impact of bed topography on hydrodynamics under a range of geometric boundaries (Blanckaert 2010; Koken & Constantinescu 2011; Konsoer *et al.* 2016; Chang *et al.* 2017). For instance, Blanckaert (2010) experimentally examined bed topographic effects on hydrodynamics in a bend channel and found that a deformed bed topography might lead to the enhancement of secondary flows and alleviation of flow shear-induced turbulence. There are few studies investigating how a deformed bed topography impacts the hydrodynamics in near-bank vegetated channels either experimentally or numerically. There are studies showing how hydrodynamics behave around a circular patch with deformed bed topography (Chang *et al.* 2017; Gu *et al.* 2018), implying that the scoured hole in the patch wake tends to inhibit the development of a vortex street.

This study aims to examine the difference in flow characteristics around near-bank vegetation over a flat bed or deformed bed. To achieve this goal, a 2D depth-averaged hydro-morphological model is employed to simulate flow and bed adjustment around a near-bank vegetation patch. Specifically, the flow motion is solved by shallow water equations with the vegetation effect modeled by the drag force method and the bed deformation solved by the Exner equation with pre-solved flow fields. One advantage of numerical modeling is to conveniently monitor the dynamic change of hydrodynamics and morphodynamics during computation. The co-evolution of hydrodynamics and morphodynamics reflect how the erodible bed immediately responds to the adjustment of the hydrodynamics, which are significant issues concerned in this study. The main objective of this study is to analyze the impact of a deformed bed on the hydrodynamics. Therefore, to stay focused, the parameter influencing the bed deformation adopted in the modeling is vegetation density. Other parameters such as patch length, patch width, water discharge and sediment size were maintained as constant and are not included in the analysis.

2. MATHEMATICAL MODEL

2.1. Model description

A 2D depth-averaged hydro-morphological model (Nay2DH, an open source code) was used to simulate flow around a near-bank vegetation patch and to simulate bed morphological evolution. The details of the hydro-morphological model were documented in the Supplementary Material. Thereby, a brief description of the model is presented here. This model incorporates a hydrodynamic module and a morphodynamic module, which are explicitly correlated with each other. The hydrodynamic module is the shallow water equations, governing the depth-averaged effect of water flow motion. To model the vegetation blockage effect on the water flow, the vegetation patch is regarded as a porous media and its effect is represented by the drag force method (a quadratic velocity law), which has been widely used in modeling vegetated flow (Choi & Kang 2006; Zeng & Li 2014; Yan *et al.* 2016; Xu *et al.* 2019). However, the turbulence arising from the vegetation stems cannot be modeled in this method, which actually is significant for sediment motion such as particle saltation (Tajnesaie *et al.* 2020).

To close the Reynolds stress terms, the standard k-ε turbulence model is used to solve the eddy viscosity for its effectiveness and stability. The sediment motion and fluvial processes are then solved by the morphodynamic module. With the flow velocities computed by the hydrodynamic module, a bed-load transport equation estimates the sediment flux, for which in this study we employ Meyer-Peter and Müller's formula. The bed deformation is solved by the Exner equation, which links the change in bed elevation to the bed-load flux in the longitudinal and transverse directions. To avoid unrealistic large-

gradient bed topography, a slope failure model based on sediment's angle of repose is used for bed deformation correction (Fischer-Antze *et al.* 2001; Jang & Shimizu 2005).

The governing equations of the flow motion and bed deformation are discretized by the finite difference method. The cubic interpolated pseudoparticle (CIP) method is mainly applied as a third-order numerical scheme, which ensures the accuracy of the numerical solution (Jang & Shimizu 2005). For the flow governing equations, at the inlet, the water discharge is specified as the inflow boundary and at the outlet a constant water depth is specified. At the sidewall, the no-slip condition is applied for flow velocities, turbulent kinetic energy and the dissipation rate. For the governing equations of morphodynamics, at the inlet, no sediment was supplied to carry out a clear water scour process which is consistent with the experiment. A detailed mathematical description can be found in Jang & Shimizu (2005) and the model manual.

2.2. Flume experiment for model validation

The validation of the hydro-morphological model was conducted by a flume experiment (Xu *et al.* 2019), which demonstrates the bed morphological change around a near-bank vegetation patch as shown in Figure 1. The bed slope was set to 1/300. The near-bank patch with a length of 2 m occupies half of the width of the flume bed with a width of 0.31 m. The patch is located in the center region of the experimental reach which is about 6 m in length. A layer of sediment with a median size of 1.42 mm was laid on the flume bottom. The layer thickness was set as 6.5 cm which is thick enough to ensure the bed being erodible during the entire scour experiment. The vegetation patch was mimicked by an array of solid cylinders, which were rectilinearly distributed. With the cylinder spacing of 0.03 m × 0.03 m, the patch density $a = 5.56\ \mathrm{m}^{-1}$. Assuming the drag coefficient $C_d = 1.2$, the drag length scale $(C_d a)^{-1} = 0.15$ m. For the experiment, the water discharge $Q = 45\ \mathrm{m}^3/\mathrm{h}$ and the downstream depth $H_d = 0.085$ m. Therefore, the averaged velocity $U = 0.474$ m/s. To direct the flow from the flat bottom to the sediment bed smoothly, a sloping gravel layer was installed in front of the sediment bed. At equilibrium of bed scour, the bed topography was measured by a point gauge in a dense grid. Acoustic Doppler Velocimetry (ADV) was used to measure flow velocity over the equilibrium bed topography for different cross-sections, as shown in Figure 1.

3. RESULTS

3.1. Model validation

The grid size ($dx = 0.1$ m and $dy = 0.01$ m) was chosen for modeling work after a grid convergence test, which can be found in the Supplementary Material. The validation of the depth-averaged hydro-morphological model was conducted by comparing the simulated flow velocities and bed topography with flume data. Figure 2(a) presents the verification with respect to the longitudinal velocities along the patch. It is apparent that the simulated flow velocities agree well with the experimental results. The average error is presented in Equation (1):

$$Er = \frac{1}{N}\sum_{1}^{N}\left|\frac{\text{simulated } U - \text{experimental } U}{\text{experimental } U}\right| \times 100\% \tag{1}$$

in which N denotes the point number of each profile. The average error ranges from 8% to 19%, with a lower error in the entrance region and higher error in the further-downstream region. This is likely because the flow along the patch gradually evolves with the generation of secondary flows, which impacts the redistribution of flow mass and momentum to lead to the difference in error. A 2D numerical model, however, is relatively poor for simulating the effect of secondary flows. Figure 2(b) shows the performance in modeling bed deformation. The simulated longitudinal bed profiles fit the measured points. In

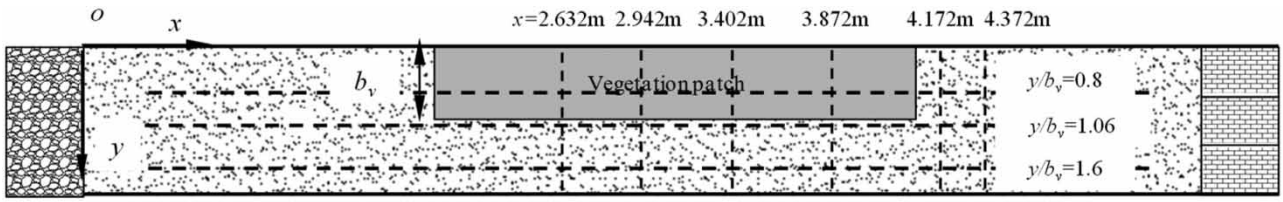

Figure 1 | Sketch of flume experiments. The dashed lines indicate the measurement profiles of velocity and bed topography for model verification.

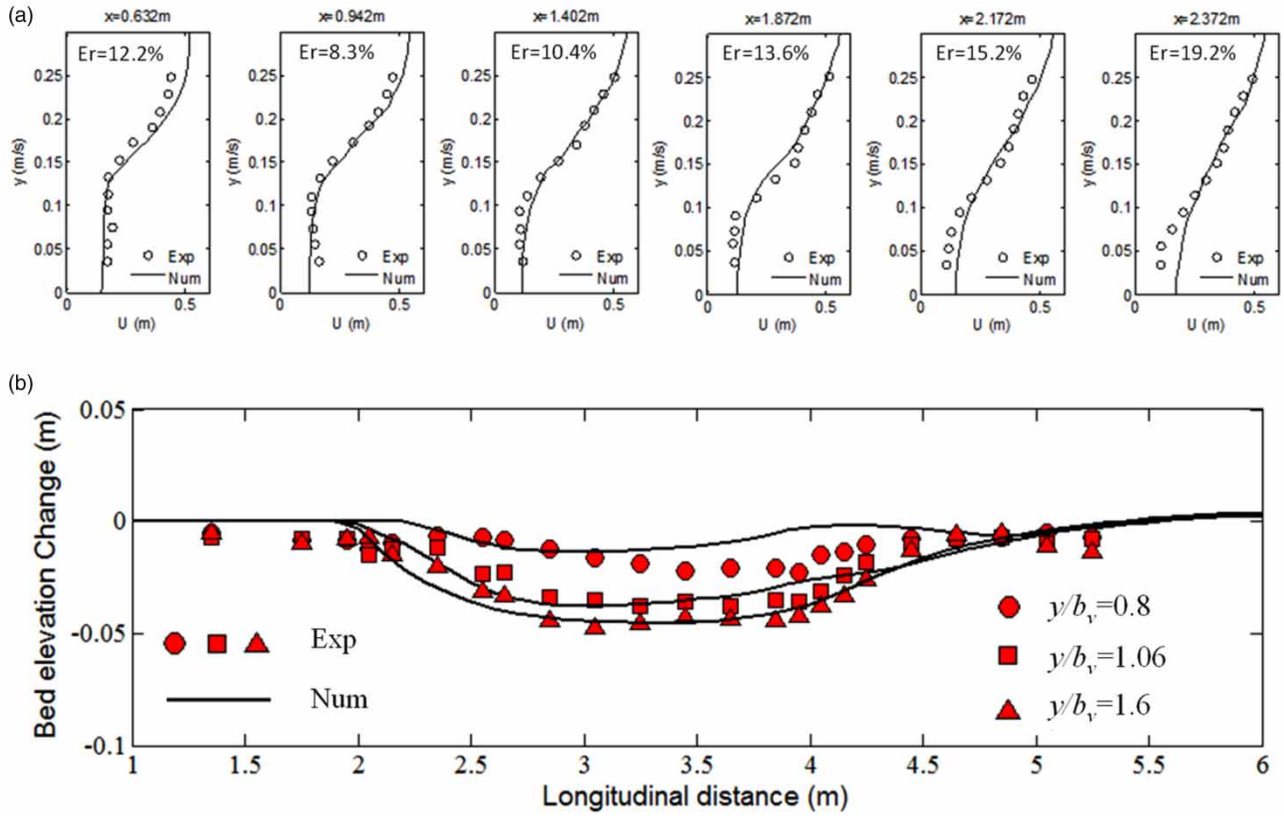

Figure 2 | Model verification for (a) longitudinal bed topography and (b) longitudinal velocity.

particular, the matching ($y/b_v = 1.06$ and 1.6) is better for the open region. For the vegetated region, the bed degradation for the downstream reach in the vegetated region is underestimated. This might be because the drag force method characterizing only the effect of individual cylinders is not sufficient to describe sediment erosion through individual cylinders. However, the simulated bed deformation for the open region is accurate, which draws more attention for research purposes in this study. Therefore, it can be said that the hydro-morphological model can generally give satisfying results, and the model is used for further analysis of the hydrodynamics over flat and deformed bed topography, which will be emphasized in the following several sections.

3.2. Bed topography characteristics

The intention of this study is to explore the impact of bed deformation on hydrodynamics in a near-bank vegetated channel. Therefore, it is better to know the bed topography characteristics under different patch densities. Figure 3 shows bed

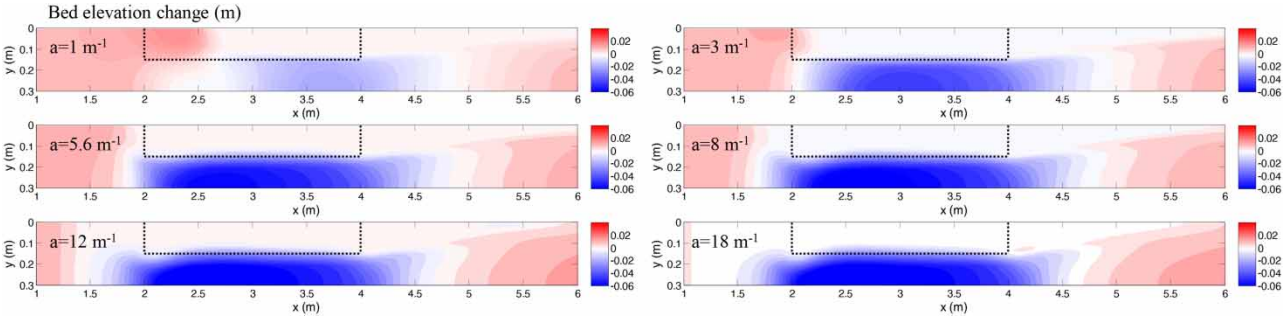

Figure 3 | Deformed bed topography around the near-bank vegetation patch under different patch densities.

topographic evolution under different patch densities starting from the same flat bed. It can be observed that as the patch density increases, the scour pool in the open region adjacent to the patch is produced and enhanced by the accelerating flow velocities and the eroded sediment tends to deposit in the downstream region. The pool enhancement occurs in both the vertical and longitudinal dimensions. For the smallest density ($a = 1\ \mathrm{m}^{-1}$), the patch exerts a lighter impact on the flow, which as a result leads to a scour pool located in the far-downstream region with the bed near the entrance less eroded. A significant finding is that as the patch density increases, the deepest area of the pool tends to expand upstream, resulting in the elongation of the scour pool. However, the longitudinal dimension of the pool is kept comparable to the patch length even if the patch density continuously increases.

3.3. Hydrodynamics over deformed bed topography: water surface, flow velocity, bed shear stress and turbulence

Knowing the bed topography characteristics under increasing patch density, we next examine how the deformed bed topography impacts the hydrodynamics. The first examined parameters are longitudinal and transverse velocities, which are shown in Figure 4. The longitudinal velocity performs an adjustment after entering the vegetated reach, with flow decelerating in the vegetated region and accelerating in the open region both for the flat bed and deformed bed. However, the bed deformation topography induces a response in the longitudinal velocity differing from that for the flat bed. Over the flat bed, the velocity for the open region continuously increases as flow propagates downstream, with the magnitude peaking in the region of the trailing edge (downstream end). Meanwhile, the velocity magnitude continuously increases with the increasing patch density but the high velocity core continues to expand upstream. Over the deformed bed, the longitudinal velocity distribution is similar to that over the flat bed with a major difference being that the longitudinal velocity is significantly reduced compared with that over the flat bed. It can be observed that the longitudinal velocity in the open region has a similar magnitude range even if the patch density increases. The decreasing velocity with the increasing patch density in the vegetated region requires an increasing net discharge in the open region to meet the mass continuity law. The larger cross-sectional area due to the deepening and elongation of the scour pool ensures the increasing net discharge without increasing the velocity. Another phenomenon is that for the deformed bed, a wider transverse transitional region links the low velocity region and high velocity region in contrast to a sharp variation for the flat bed. Moreover, the transitional band is wider for a larger patch density.

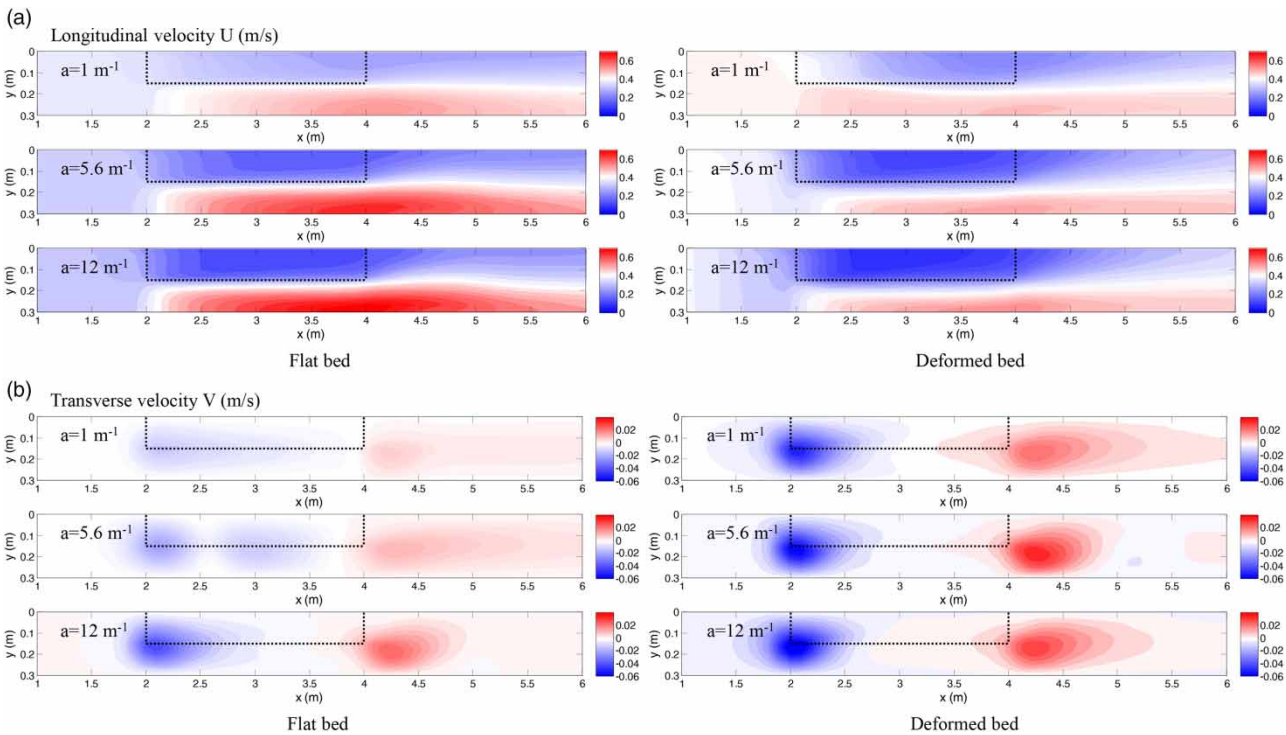

Figure 4 | Fully-developed transverse velocity around the near-bank vegetation patch for a flat bed and deformed bed.

For the transverse velocity for the flat bed (Figure 4(b)), negative and positive zones occur near the leading edge and trailing edge, reflecting the flow convergence and divergence behavior corresponding to the presence of the near-bank patch. The increasing patch density enhances the magnitude of the two zones for the flat bed. For the deformed bed, a more pronounced transverse flow motion can be observed even over a minor deformed bed for the smallest patch density. Likewise, a larger patch density induces more enhanced transverse flow motion but the enhancement might be lighter than that for the flat bed. The pronounced transverse motion indicates that the bed deformation may enhance the effect of the secondary flows evolving along the patch, which was found in the channel occupied by a near-bank patch. Of interest is that for both the flat bed and deformed bed, the positive velocity zone near the trailing edge transforms from a long pattern to a short one as the patch density increases, indicating that the flow separation effect gets more pronounced.

Due to the blocking of the vegetation patch, the momentum is redistributed spatially due to the contribution of different hydrodynamic effects. In between, the effect of the hydraulic pressure gradient characterized by the water surface gradient plays an essential role. For the flat bed, the longitudinal surface gradient ($S_x = \partial z_s/\partial x$) becomes pronounced for the vegetated reach (Figure 5(a)). This is attributed to outstanding vegetative resistance, which is partially balanced by the force due to the positive hydraulic pressure gradient. Under a small density ($a = 1\ \mathrm{m}^{-1}$), the water surface gradient tends to be uniform along the patch. As the patch density increases, a higher magnitude core appears in the entrance region of the patch. This might be because the entrance energy work consumed by the patch related to velocity loss is more pronounced for a larger density. Furthermore, the high core diffuses to the adjacent open region with a light decay, which is more pronounced for a larger density. For the deformed bed, the longitudinal water surface gradient is generally lower than that for the flat bed. However, it can be observed that the distribution pattern is similar to that for the flat bed. The sloping bed topography may account for this decay effect. Interestingly, negative value arises in front of the vegetated reach for the deformed bed, which is negligible for the flat bed.

Compared with the longitudinal component, the transverse surface gradient ($S_x = \partial z_s/\partial x$) performs similarly for the flat bed and deformed bed (Figure 5(b)). At the entrance, a positive-negative zone is distributed in an orderly way. The first positive zone indicates that the hydraulic pressure may drive transverse flow motion toward the open region and the incipient transverse motion of sediment from the vegetated zone to the open zone. The pattern of the transverse surface gradient

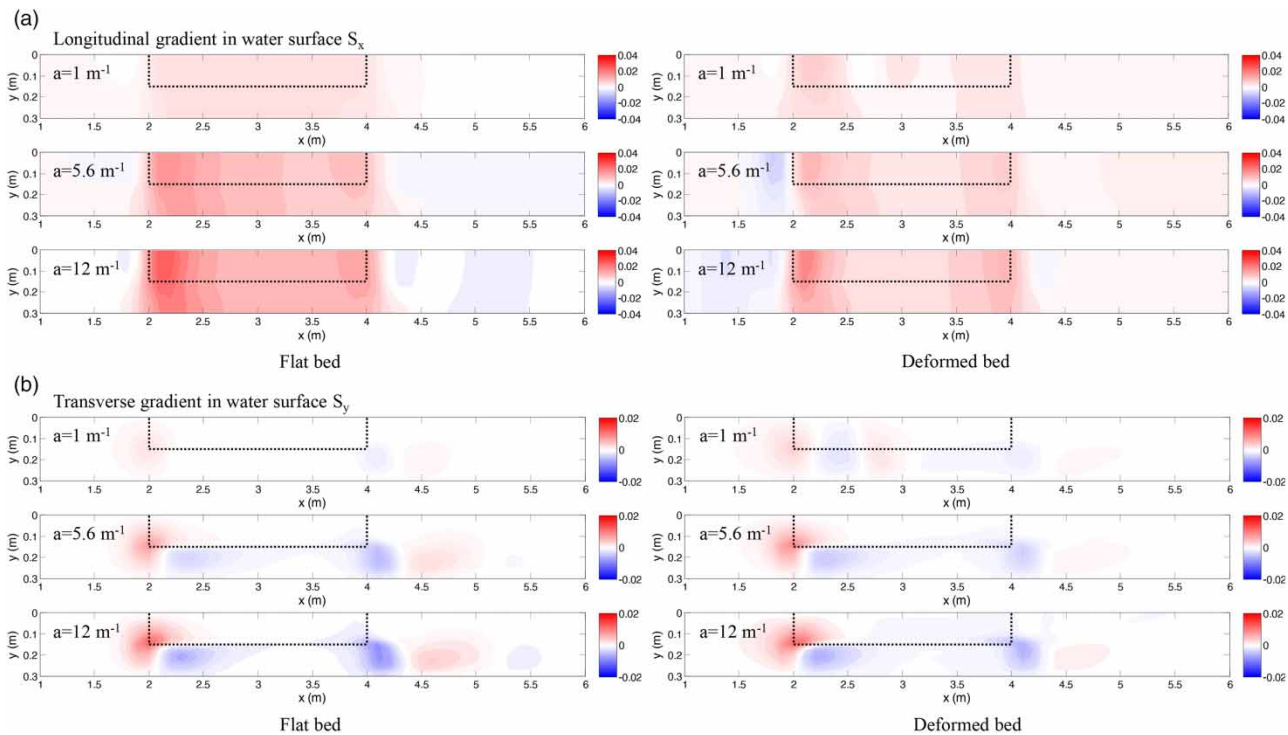

Figure 5 | Surface gradient in the (a) longitudinal and (b) transverse directions around the near-bank vegetation patch for a flat bed and deformed bed.

well corresponds to the transverse velocity. Downstream of the exit, a negative-positive zone pair is also distributed in an orderly way. The first negative zone corresponds to the flow separation in the patch wake, which may also partially contribute to the transverse motion of sediment toward the patch wake. Furthermore, the effect of the transverse surface gradient pattern is enhanced as the patch density increases.

The distribution of the bed shear stress around the patch impacts the sediment motion and stable bed topography (Figure 6). For the flat bed, the bed shear stress concentrates in the open region near the trailing edge similar to the pattern of longitudinal velocity, indicating the most erodible area. The bed shear stress in the vegetated region decreases greatly due to vegetation resistance. As the patch density increases, the zone of concentrated bed shear stress tends to expand both upstream and downstream. However, the concentrated zone for the initial condition is not consistent with the orientation of the scour pool at equilibrium under a larger patch density, indicating that the bed shear stress redistributes during the bed topographic adjustment. After the bed topography adjustment is completed, the bed shear stress distribution performs a distinct pattern. The bed shear stress in the vegetated zone only differs slightly from that for the flat bed. This is because the bed in the vegetated zone is maintained well by the vegetation without apparent bed deformation. The concentrated bed shear stress in the open region, however, greatly decreases as the bed is eroded. This can be explained by the fact that the excessive bed shear stress vanishes as the upper-layer sediment is eroded. A larger patch density still leads to higher bed shear stress. This is because the more sloping bed topography exerting a topographic effect on sediment under a larger patch density requires larger critical shear stress to drive the incipient motion of sediment compared with uniform flow.

The partial blocking of the near-bank patch produced a low-velocity zone in the vegetated region and a high-velocity zone in the open region, which produced a significant flow shear along the interface. The flow shear inducing the flow instability gives rise to horizontal coherent vortices. The vortices can be well quantified by the vorticity ($= \partial U/\partial y - \partial V/\partial x$), which is shown in Figure 7. For the flat bed, the vorticity arises from the junction interface after the flow entering the vegetated reach and laterally develops along the patch until the trailing edge, indicating continuous development of horizontal coherent vortices. The increasing patch density promoting the flow shearing is likely to produce a pronounced vorticity field. The above

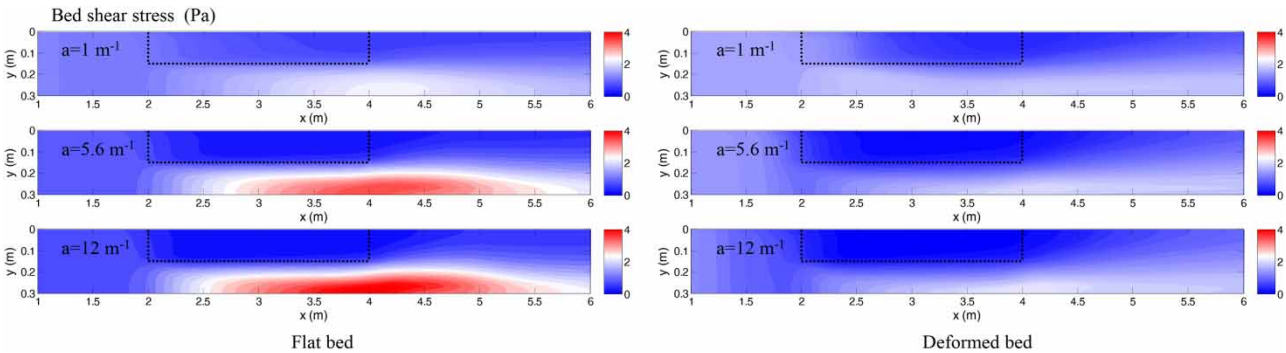

Figure 6 | Fully-developed bed shear stress around the near-bank vegetation patch for a flat bed and deformed bed.

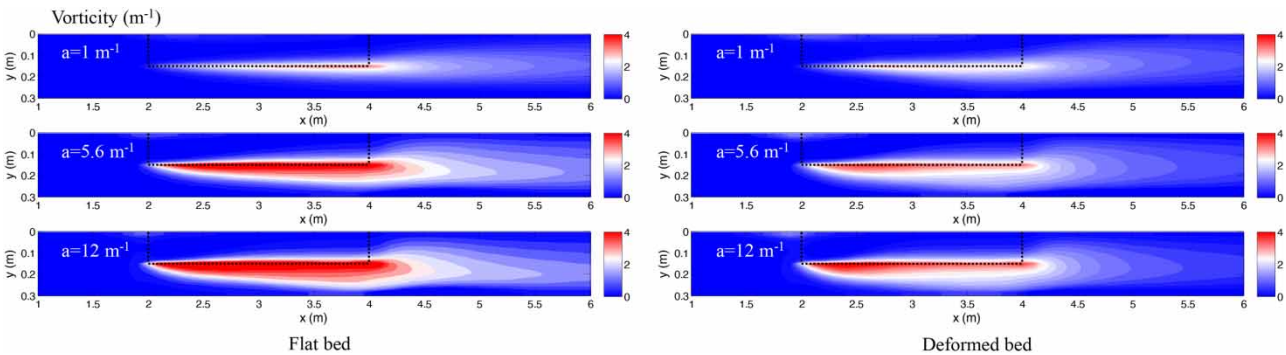

Figure 7 | Fully-developed vorticity around the near-bank vegetation patch for a flat bed and deformed bed.

results are well consistent with previous studies by both experiments and simulations (White & Nepf 2007; Huai *et al.* 2015). For the deformed bed, the spatial vorticity pattern totally changes compared with that for the flat bed. First, it was found that the magnitude of vorticity for the deformed bed is generally lower than that for the flat bed. This is consistent with the reduced longitudinal velocity for the deformed bed (see Figure 4(a)). Unlike the continuous development of the vorticity along the patch for the flat bed, a wider significant zone of the vorticity is reached near the entrance region and then the significant zone continues to shrink along the patch. The transformed pattern of vorticity indicates that the bed deformation tends to alleviate the turbulent extent by reducing the effect of the flow shearing. As compensation, the secondary flows indicated by enhanced transverse flow motion (see Figure 4(b)) might play an outstanding role in the exchange of mass and momentum.

4. DISCUSSION

The verified 2D hydro-morphological model allows a deep analysis of the impact of bed deformation on hydrodynamics. The presentation of hydrodynamics over the flat bed acting as reference allows a better understanding of the effect of the deformed bed topography. When a patch of vegetation partially occupies the channel bed, the hydrodynamics firstly adjust due to the spatial balance between the individual components of momentum. Flow velocity shows a characteristic pattern regarding both the longitudinal and transverse velocity. The longitudinal velocity decelerates for the vegetated region and accelerates for the open region and peaks near the trailing edge for the flat bed, which is closely related to the distribution of bed shear stress. The distribution of longitudinal velocity and bed shear stress indicates that the bed erosion in the open region initiates near the trailing edge of the patch. For a small patch density ($a = 1\ \mathrm{m}^{-1}$), the deepest area of the scour pool is consistent with that of bed shear stress. However, as the patch density increases, the deepest area of the scour pool expands upstream, differing from the patterns of the longitudinal velocity and bed shear stress for the flat bed. Interestingly, the elongated pool profile varies consistently with the distribution of the longitudinal velocity and bed shear stress for the deformed bed, the magnitudes of which, however, are significantly reduced.

With the bed topography being deformed, the growth in longitudinal velocity in the lateral direction is developed with a larger width at the downstream of the vegetated reach (See Figure 4(a)); and this effect is enhanced as the pool is deepened by the increase in patch density. This suggests that the lateral development of the longitudinal velocity is attributed to the transverse sloping bed topography. An extreme scenario is that for the flat bed the lateral development of longitudinal velocity has a sharp transition near the junction. For a flat bed, the transverse growth of the longitudinal velocity or flow mixing is impacted by the generated horizontal coherent vortices indicated by vorticity (Nepf (2012) stated that for a flat bed horizontal vortices form for $ah > 0.1$, where $h =$ water depth). The distribution of the vorticity along the junction for the deformed bed is much lower than that for the flat bed. Therefore, the above statements indicate that the deformed bed, by reducing the velocity in the open region, diminishes the shear effect (mixing) in the junction region but exerts a topographic effect to enhance the transverse flow mixing. The essential cause is thought to be that the bed topographic effect might enhance the effect of secondary flow, which is likely to exceed the mixing effect induced by horizontal vortices. The increased depth-averaged transverse velocity around the patch might support this thought (see Figure 4(b)). Strong secondary flows are commonly present over deformed bed topography such as compound beds (Kang & Choi 2006; Yang *et al.* 2007).

The 2D depth-averaged model cannot simulate the generation of the secondary flow evolving along the patch, which has been found in flume experiments and numerical simulations (Nezu & Onitsuka 2001; Choi & Kang 2006). Some hydrodynamic parameters, however, (for instance, transverse velocity and transverse surface gradient) can indicate its formation. For either a flat bed or deformed bed, pronounced transverse surface gradient occurs as the flow encounters the patch. The positive value indicating hydraulic pressure head tends to drive the transverse flow motion from the patch to the open region, which is confirmed by the negative transverse velocity (see Figure 4(b)). As the patch density increases, the surface gradient and transverse motion both become more pronounced so that secondary flows are most likely to be triggered. However, when the bed is deformed, the transverse flow motion near the leading edge is enhanced despite the fact that the surface gradient is reduced. The transverse motion for the deformed bed is negatively contributed by the reduced surface gradient but more positively enhanced by the sloping bed topography. Therefore, the deformed bed topography is expected to induce more intense secondary flows compared with those for the flat bed. The secondary flows induce transverse momentum exchange and thus can promote the flow adjustment.

Previous studies show that the interior adjustment of flow in the vegetated region is related to the blocking effect, characterized by the patch drag length ($(C_d a)^{-1}$) and patch width (b_v). Rominger & Nepf (2011), based on scale analysis and experimental data, proposed a quantitative formula (Equation (2)) to describe such a relation, i.e.:

$$L_a = (3.0 \pm 0.3)\left[\frac{2}{C_d a}(1 + (C_d a b)^2)\right] \tag{2}$$

Likely, it is worth examining how the deformed bed topography impacts the interior flow adjustment. Figure 8(a) shows the longitudinal variation of the longitudinal velocity in the vegetated region ($y/b_v = 0.25$) as the patch density increases for the flat bed and deformed bed. The full adjustment of flow is estimated by the velocity which varies by less than 5%. It can be

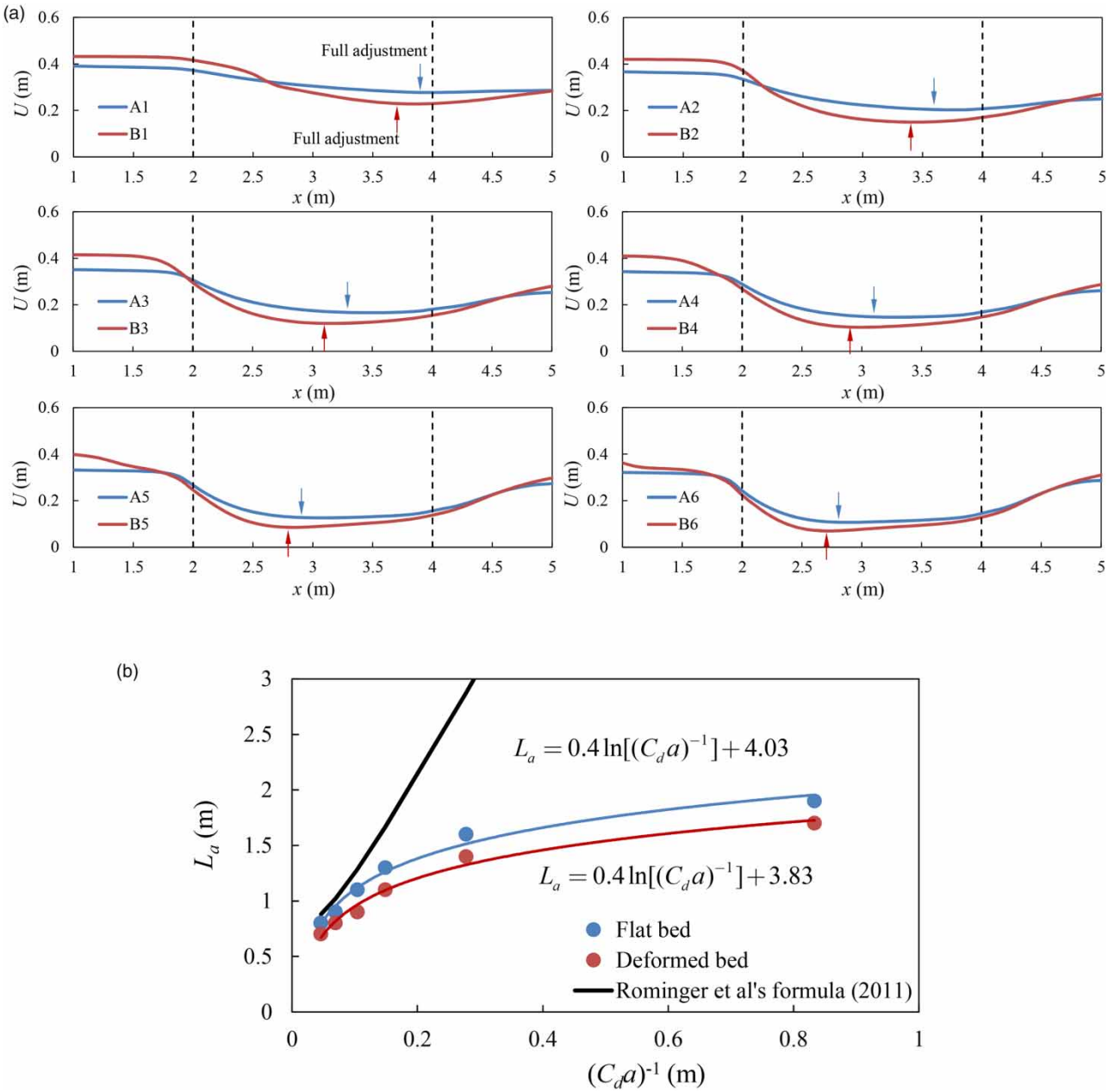

Figure 8 | (a) Interior adjustment of the longitudinal velocity in the vegetation region for the flat bed and deformed bed and (b) relation between the flow adjustment distance and drag length for the flat bed and deformed bed.

clearly observed that for all scenarios the full adjustment of flow (regarding the longitudinal velocity) for the flat bed needs a longer distance (L_a). The increasing patch density (negatively related to $(C_d a)^{-1}$) leads to a further decrease in the distance of full flow adjustment for both the flat bed and deformed bed, agreeing well with the observed results by previous studies. By plotting the drag length and longitudinal velocity, the two sets of data for the flat bed and deformed bed can be well described by a logarithmic formula, respectively, as shown in Figure 8(b). Interestingly, the two formulas differ from each other only by a difference of 0.2. In other words, the interior flow adjustment distance for the deformed bed is shorter than that for the flat bed by an intersect of 0.2, systematically. However, the obtained relation greatly deviates from the proposed formula by Rominger & Nepf (2011) in terms of low patch density (high $(C_d a)^{-1}$). This might be because the setting patch length for sparse vegetation is insufficient for the interior full adjustment of flow.

5. CONCLUSIONS

The growth of near-bank vegetation is likely to induce the adjustment of both hydrodynamics and surrounding bed topography. How the deformed bed topography impacts hydrodynamics determines bed stability, future fluvial evolution and the ecological effect. Furthermore, the existing knowledge for near-bank vegetated flows for flat beds may bring uncertainty for a deformed bed. However, this important issue has been rarely addressed by existing studies. The present study conducts a numerical investigation of the impact of a deformed bed topography on hydrodynamics in an open channel occupied by a near-bank vegetation patch. The strategy of this study is to first verify the 2D hydro-morphological model with the hydrodynamics and topography of a deformed bed in a laboratory flume and to secondly apply the model to conduct bed scour numerical experiments under a variety of patch densities. The following summary can be drawn from the simulated results:

(1) The simulation shows that the deepest area of the scour pool adjacent to the patch expands upstream as the patch density increases. However, the longitudinal velocity and bed shear stress for the flat bed (before the initiation of bed scour) peaking near the trailing edge of the patch indicate the bed shear stress continuously adjusts during the scour process.
(2) The formation of a deformed bed topography leads to a significant reduction of the longitudinal velocity and bed shear stress. The transverse motion of flow near the leading edge and trailing edge indicating flow convergence and divergence, however, is apparently enhanced, which may strengthen the secondary flows along the patch. The deformed bed topography apparently alleviates the longitudinal water surface gradient but has a lighter effect on the transverse surface gradient.
(3) The vorticity arising from coherent vortices along the junction between the patch and adjacent open region is strongly inhibited by a deformed bed topography compared with that for a flat bed. This indicates that a deformed bed topography can reduce the extent of turbulence and flow mixing between the vegetated region and open region. Alternatively, the secondary flows generated in the open region can compensate for the flow mixing effect of the reduced turbulence.
(4) We studied the flow adjustment over a deformed bed topography and found that the interior adjustment distance regarding the longitudinal velocity is shortened due to the presence of the bed topography. This phenomenon can be explained by the effect of the sloping bed topography near the entrance of the vegetated reach. A logarithmic relation is found to exist between the adjustment distance and vegetative drag length, which deviates from the formula proposed by previous studies in terms of sparse vegetation. The shortening of flow adjustment distance by the deformed bed topography is also suggested by the redistribution of the net water discharge for the vegetated region and open region.

However, the gained results should be applied with caution due to the scale effect of the flume. Comparably, the flume scale is more likely to occur in a high-gradient mountainous stream, which is often characterized by narrow width and relatively small aspect ratio (width-to-depth ratio). This also sets the research direction for near-bank vegetated hydrodynamics. Furthermore, the hydro-morphological model used, which cannot consider the turbulence arising from vegetation stems, might underestimate sediment transport in the vegetation region.

ACKNOWLEDGEMENTS

This research was supported by the National Key R&D Program of China (2018YFC0407801) and the National Natural Science Foundation of China (51909178 and 51809107).

DATA AVAILABILITY STATEMENT

Data cannot be made publicly available; readers should contact the corresponding author for details.

REFERENCES

Blanckaert, K. 2010 Topographic steering, flow recirculation, velocity redistribution, and bed topography in sharp meander bends. *Water Resources Research* **46** (9), doi:10.1029/2009WR008303.

Chang, W.-Y., Constantinescu, G. & Tsai, W. F. 2017 On the flow and coherent structures generated by a circular array of rigid emerged cylinders placed in an open channel with flat and deformed bed. *Journal of Fluid Mechanics* **831**, 1–40.

Choi, S.-U. & Kang, H. 2006 Numerical investigations of mean flow and turbulence structures of partly-vegetated open-channel flows using the Reynolds stress model. *Journal of Hydraulic Research* **44** (2), 203–217.

Fischer-Antze, T., Stoesser, T., Bates, P. & Olsen, N. 2001 3D numerical modelling of open-channel flow with submerged vegetation. *Journal of Hydraulic Research* **39** (3), 303–310.

Ghaderi, A., Daneshfaraz, R., Torabi, M., Abraham, J. & Azamathulla, H. M. 2020 Experimental investigation on effective scouring parameters downstream from stepped spillways. *Water Supply* **20** (5), 1988–1998.

Gu, J., Shan, Y., Liu, C. & Liu, X. 2018 Feedbacks of flow and bed morphology from a submerged dense vegetation patch without upstream sediment supply. *Environmental Fluid Mechanics* **19**, 475–493. https://doi.org/10.1007/s10652-018-9633-5.

Huai, W., Xue, W. & Qian, Z. 2015 Large-eddy simulation of turbulent rectangular open-channel flow with an emergent rigid vegetation patch. *Advances in Water Resources* **80**, 30–42.

Jang, C.-L. & Shimizu, Y. 2005 Numerical simulation of relatively wide, shallow channels with erodible banks. *Journal of Hydraulic Engineering* **131** (7), 565–575.

Kang, H. & Choi, S.-U. 2006 Turbulence modeling of compound open-channel flows with and without vegetation on the floodplain using the Reynolds stress model. *Advances in Water Resources* **29** (11), 1650–1664.

Kim, H. S., Kimura, I. & Shimizu, Y. 2015 Bed morphological changes around a finite patch of vegetation. *Earth Surface Processes and Landforms* **40** (3), 375–388.

Koken, M. & Constantinescu, G. 2011 Flow and turbulence structure around a spur dike in a channel with a large scour hole. *Water Resources Research* **47** (12).

Konsoer, K. M., Rhoads, B. L., Best, J. L., Langendoen, E. J., Abad, J. D., Dan, R. P. & Garcia, M. H. 2016 Three-dimensional flow structure and bed morphology in large elongate meander loops with different outer bank roughness characteristics. *Water Resources Research* **52** (12), 9621–9641.

Nepf, H. M. 2012 Hydrodynamics of vegetated channels. *Journal of Hydraulic Research* **50** (3), 262–279.

Nezu, I. & Onitsuka, K. 2001 Turbulent structures in partly vegetated open-channel flows with LDA and PI V measurements. *Journal of Hydraulic Research* **39** (6), 629–642.

Rominger, J. T. & Nepf, H. M. 2011 Flow adjustment and interior flow associated with a rectangular porous obstruction. *Journal of Fluid Mechanics* **680**, 636–659.

Santos, J. M., Branco, P., Katopodis, C., Ferreira, T. & Pinheiro, A. 2014 Retrofitting pool-and-weir fishways to improve passage performance of benthic fishes: effect of boulder density and fishway discharge. *Ecological Engineering* **73**, 335–344.

Tajnesaie, M., Jafari Nodoushan, E., Barati, R. & Azhdary Moghadam, M. 2020 Performance comparison of four turbulence models for modeling of secondary flow cells in simple trapezoidal channels. *ISH Journal of Hydraulic Engineering* **26** (2), 187–197.

White, B. L. & Nepf, H. M. 2007 Shear instability and coherent structures in shallow flow adjacent to a porous layer. *Journal of Fluid Mechanics* **593**, 1–32.

Xu, M.-Z., Wang, Z.-Y., Pan, B.-Z. & Na, Z. 2012 Distribution and species composition of macroinvertebrates in the hyporheic zone of bed sediment. *International Journal of Sediment Research* **27** (2), 129–140.

Xu, Z.-X., Ye, C., Zhang, Y.-Y., Wang, X.-K. & Yan, X.-F. 2019 2D numerical analysis of the influence of near-bank vegetation patches on the bed morphological adjustment. *Environmental Fluid Mechanics* **20** (12), 707–738.

Yan, X.-F., Wai, W.-H. O. & Li, C.-W. 2016 Characteristics of flow structure of free-surface flow in a partly obstructed open channel with vegetation patch. *Environmental Fluid Mechanics* **16** (4), 807–832.

Yang, S. L., Zhang, J. & Xu, X. 2007 Influence of the Three Gorges Dam on downstream delivery of sediment and its environmental implications, Yangtze River. *Geophysical Research Letters* **34** (10).

Zeng, C. & Li, C. W. 2014 Measurements and modeling of open-channel flows with finite semi-rigid vegetation patches. *Environmental Fluid Mechanics* **14** (1), 113–134.

Zhao, N., Wang, Z. Y., Pan, B. Z., Xu, M. Z. & Li, Z. W. 2015 Macroinvertebrate assemblages in mountain streams with different streambed stability. *River Research and Applications* **31** (7), 825–833.

First received 6 July 2021; accepted in revised form 14 September 2021. Available online 29 September 2021